# Mechanical behavior of ultralow-dielectric-constant mesoporous amorphous silica

M. Rauf Gungor, James J. Watkins, and Dimitrios Maroudas

Citation: Applied Physics Letters **92**, 251903 (2008); doi: 10.1063/1.2949556
View online: http://dx.doi.org/10.1063/1.2949556
View Table of Contents: http://scitation.aip.org/content/aip/journal/apl/92/25?ver=pdfcov
Published by the AIP Publishing

# Mechanical behavior of ultralow-dielectric-constant mesoporous amorphous silica

M. Rauf Gungor,[1] James J. Watkins,[1,2] and Dimitrios Maroudas[1,a)]
[1]*Department of Chemical Engineering, University of Massachusetts Amherst, Amherst, Massachusetts 01003-3110, USA*
[2]*Department of Polymer Science and Engineering, University of Massachusetts Amherst, Amherst, Massachusetts 01003-3110, USA*

(Received 9 April 2008; accepted 3 June 2008; published online 23 June 2008)

Using molecular-dynamics simulations, we examine the mechanical behavior of mesoporous amorphous silicas that are considered as ultralow-dielectric-constant materials in microelectronics. We study structures with a regular array of spherical pores and densities between 88% and 72% of the amorphous silica normal density. We find that the Young modulus depends on density according to a sublinear power-law scaling relationship and decreases with decreasing mesopore size. Upon uniaxial compression, an elastic instability is triggered in structures with less-than-critical density or mesopore size. © *2008 American Institute of Physics*. [DOI: 10.1063/1.2949556]

In present generations of high-performance microelectronic devices, the number of transistors is approaching the order of billions, as facilitated by increasingly high levels of integration in semiconductor technologies. These transistors are interconnected through copper wiring embedded in multiple layers of insulating dielectric material, which is traditionally silicon dioxide. Increasing integration scales leads to closer spacing between interconnect lines and requires a lower dielectric constant (low-$k$) of the dielectric material in order to reduce the capacitive coupling between the interconnect lines. All candidates for ultralow-$k$ materials must also satisfy certain integration requirements, such as a minimum mechanical strength, threshold of thermal and electrical breakdown, and suitability for lithographic processing during chip manufacturing.[1] Mechanical strength is particularly important to ensure the structural integrity of the device under the thermomechanical loading conditions characteristic of semiconductor manufacturing processes, chip packaging, and device service. Among materials considered for ultralow-$k$ applications, porous amorphous silicas are particularly appealing due to their compatibility with current semiconductor manufacturing technologies.[2–5]

Decreasing the material's density for lowering its dielectric constant causes the mechanical properties of porous amorphous silicas to deteriorate.[6] Computational studies based on large-scale molecular-dynamics (MD) simulations of the fracture mechanics of amorphous silica demonstrated growth and healing of wing cracks in confined silica glass under dynamic compression[7] and investigated the interaction of voids in silica glass under hydrostatic tension.[8] MD simulations also have been used to investigate the structure of porous silica and the transformation from a dense to a microporous amorphous structure.[9] In addition, atomic-scale computational studies have demonstrated the stoichiometry breaking by migration of nonbridging oxygen atoms to the free surface of amorphous silica and its relation to the nonuniform mechanical properties in the material.[10] In spite of these advances, a fundamental understanding of the structural response to loading of ordered mesoporous amorphous silica structures is still lacking and the dependence of their mechanical properties on density and pore size remains elusive.

The purpose of this letter is to gain a fundamental understanding of the mechanical behavior and analyze the mechanical properties and structural stability of amorphous silica materials with nanometer-scale pores as a function of their density and pore size. Using MD simulations, we generate mesoporous amorphous silica structures with regular arrays of spherical pores and examine their mechanical strength and structural response to straining. We vary the overall density by varying two parameters: pore diameter and pore center-to-center distance. Variation of the overall film density in synthetic systems may also be possible by varying either the degree of subnanometer-scale porosity in pore walls, while maintaining the mean pore size and spacing,[3] or the void fraction of mesopores through varying porogen concentration,[11] or the size of the mesopores via the choice of template.[12] Our simulation scheme can examine each of these scenarios.

Our MD simulations were based on a realistic many-body interatomic potential for silica.[13,14] The velocity-Verlet method[15] was employed to integrate the classical equations of motion with a time step of 0.5 fs. Unless otherwise specified, the simulations were conducted under constant temperature and strain (or volume). To generate the normal-density amorphous silica ($a$-$SiO_2$) structure, we started from a cubic simulation supercell with dimensions $86\times86\times86$ Å$^3$ containing 41 472 atoms of Si and O in the stoichiometric proportion for $SiO_2$ and arranged according to the $\beta$-cristobalite structure. This initial configuration was heated from 300 to 5000 K in 30 000 time steps, followed by annealing at 5000 K for 40 000 time steps. During heating to and annealing at 5000 K, a structural order parameter based on the geometric structure factor was monitored in order to verify that an order-to-disorder transition occurred upon melting. After annealing at 5000 K, the $SiO_2$ melt was cooled down to 300 K in 50 000 time steps, and then annealed at 300 K for another 50 000 time steps. Both annealing stages, at 5000 and 300 K, were sufficiently long to ensure thermal equilibration and structural relaxation. After annealing at 300 K, uniform volume relaxation was carried out dynamically by gradually reducing the supercell volume at 300 K. This accounted for the volume contraction upon amorphization of

a)Author to whom correspondence should be addressed. Electronic mail: maroudas@ecs.umass.edu.



 

the initial $\beta$-cristobalite structure. Finally, the volume-relaxed configuration was thermally equilibrated for 30 000 time steps at 300 K and at the minimum-energy volume.

We have monitored the Si–O, O–O, and Si–Si pair correlation functions $g(r)$ of the normal-density $a$-$SiO_2$ structure after volume relaxation and subsequent thermal equilibration. The long-range order has been completely lost and the average Si–O bond length is 1.55 Å. In the initial perfectly stoichiometric $\beta$-cristobalite $SiO_2$ structure, all of the Si atoms have a coordination number $Z=4$. After annealing at 5000 K, the concentration of fourfold coordinated Si atoms is reduced to 77%, while the concentration of threefold coordinated, $Z=3$, and fivefold coordinated, $Z=5$, Si atoms increases to 20% and 3%, respectively. Upon cooling to 300 K and equilibrating, the majority of the coordination defects created at high temperature are annealed: 94%, 5%, and 1% of the Si atoms have $Z=4$, 3, and 5, respectively. Subsequently, upon volume relaxation of the annealed $a$-$SiO_2$, the corresponding energy minimum is reached after the volume is compressed uniformly by 7.8%.

This normal-density $a$-$SiO_2$ structure was then used to create the mesoporous amorphous silica structures at densities of 88%, 82%, 77%, and 72% of the normal density $\rho_0$ with spherical pore diameters $d=10$, 5, 2.5, 1.67, and 1.25 nm. The spherical pores were arranged in a simple cubic lattice, with given $d$ and interpore distance. Each pore was created by removal of atoms to form a spherical void volume inside the $a$-$SiO_2$ supercell. The density $\rho$ of the mesoporous structure is determined by $d$ and the center-to-center distance of two nearest-neighbor spherical pores (simple cubic lattice parameter). After the spherical pore generation, the resulting mesoporous structures were annealed at 300 K for 20 000 time steps, which was sufficient for their thermal equilibration and structural relaxation. These structures were then tested under uniaxial compressive strain at 300 K. The strain was applied through supercell edge size reduction along a given direction up to a level $\varepsilon=2\%$ at a rate of $4\times10^{10}$ $s^{-1}$. Subsequently, the material was equilibrated thermally at 300 K and $\varepsilon=2\%$ for 45 000 time steps. The Young modulus $M$ of the mesoporous $a$-$SiO_2$ structure was calculated according to the relation $\Delta E=M\varepsilon^2/2$, where $\Delta E$ is the elastically stored energy (potential energy difference between the strained and unstrained states) during the uniaxial compressive straining stage for dynamic straining of the material up to strain level $\varepsilon$. Careful tests confirmed that a maximum strain level of 2% does not cause plastic deformation or fracture during the dynamic straining period.

Figure 1 shows representative atomic configurations of ordered mesoporous $a$-$SiO_2$ structures with spherical pores, at various densities and pore diameters, after the application of dynamic uniaxial compressive straining up to $\varepsilon=2\%$ and subsequent isostrain (at $\varepsilon=2\%$) thermal equilibration. The configurations depict an 8-Å-thick slice of the simulation cell around a {001} plane of the simple cubic lattice of the spherical pores, which passes through the pore centers. The direction of the applied uniaxial straining is the ⟨001⟩ direction normal to this {001} plane. Specifically, Fig. 1(a) shows the response to compressive straining of mesoporous $a$-$SiO_2$ structures at constant density, $\rho=0.88\rho_0$, as a function of spherical pore diameter $d$ over the range $1.25\leqslant d\leqslant5$ nm. The first three mesoporous materials shown are structurally stable, while the fourth one, $d=1.25$ nm, is structurally unstable. In Fig. 1(b), the structural response is shown at a constant pore size, $d=2.5$ nm, as a function of $\rho$ over the range $0.72\leqslant\rho/\rho_0\leqslant0.88$. The first two materials shown are structurally stable, while the remaining two, $\rho/\rho_0=0.77$ and 0.72, are structurally unstable. In both cases, Figs. 1(a) and 1(b), the structural instability is the outcome of a smaller-than-critical wall thickness. The wall thickness is defined as the minimum thickness of the $a$-$SiO_2$ material separating adjacent pores and its critical level is reached as $\rho$ decreases at given $d$ or $d$ decreases at given $\rho$. In all the cases of unstable structural response, the instability is facilitated by the severance of the walls that separate adjacent pores, which leads to pore coalescence and, eventually, to rupture.

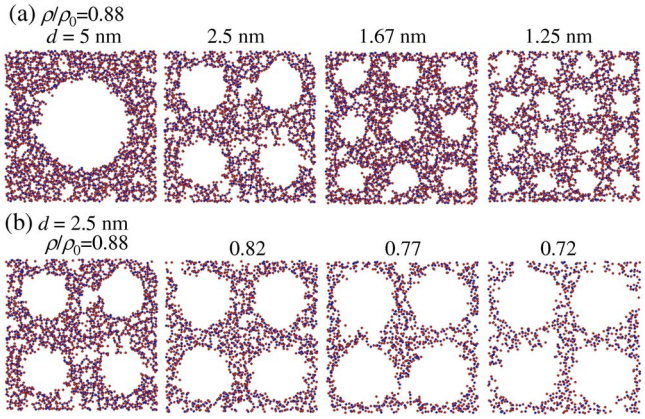


FIG. 1. (Color online) Atomic configurations of ordered mesoporous $a$-$SiO_2$ structures with spherical pores after application of dynamic uniaxial compressive straining up to $\varepsilon=2\%$ and subsequent isostrain thermal equilibration. The configurations depict an 8-Å-thick slice of the supercell around a {001} plane of the simple cubic lattice of the spherical pores that passes through the pore centers. Configurations are shown at (a) constant density, $\rho/\rho_0=0.88$, for pore diameters $d=5$, 2.5, 1.67, and 1.25 nm and (b) at constant pore diameter, $d=2.5$ nm, for densities $\rho/\rho_0=0.88$, 0.82, 0.77, and 0.72.

The dependence of the Young modulus $M$ on $d$ and $\rho$ for our MD-generated mesoporous $a$-$SiO_2$ structures is shown in Fig. 2. Our procedure for the modulus computation is highlighted in the inset to Fig. 2(a), which depicts the elastically stored energy $\Delta E$ as a function of strain $\varepsilon$ during the dynamic uniaxial compressive straining stage, $\varepsilon=\dot{\varepsilon}t$, where $\dot{\varepsilon}$ is the constant strain rate applied at this stage leading to an increase in $\varepsilon$ from 0% to 2%. The cases shown in the inset are for the normal-density $a$-$SiO_2$ structure and for the $d=2.5$ and 1.25 nm mesoporous structures at $\rho/\rho_0=0.88$. In all cases except for $d=1.25$ nm, $\Delta E$ increases during the dynamic straining stage (the initial 0.5 ps period). For $d=1.25$ nm, however, $\Delta E$ decreases (until it reaches a minimum) during this stage, which corresponds to a negative elastic modulus and implies an elastic instability.[16] The smooth curves shown in the inset correspond to quadratic polynomial fits to the MD results for $\Delta E(\varepsilon)$. The perfect fits confirm the purely linearly elastic mechanical response of the mesoporous structures during the dynamic straining period and guarantee the accurate calculation of the Young modulus, $M$.

For the normal-density $a$-$SiO_2$ structure, we calculate a modulus $M_0=125$ GPa. The inset to Fig. 2(b) shows the density dependence of the calculated (open circles) Young moduli, $M$, for the mesoporous structures with $d=10$ nm in a logarithmic plot of $M/M_0$ (shifted by a constant value) as a function of $\rho/\rho_0$. The straight line is a fit to the MD predic-

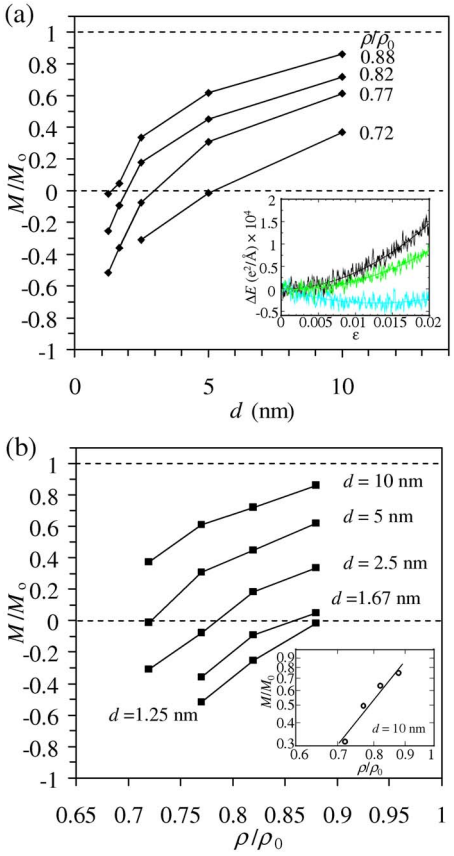


FIG. 2. (Color online) Calculated $M/M_0$ (solid squares) as (a) a function of $d$ at various densities, $\rho/\rho_0$, and (b) a function of $\rho/\rho_0$ at various pore diameters, $d$. The inset in (a) shows the elastically stored energy per atom $\Delta E$ as a function of strain during dynamic uniaxial compressive straining for the normal-density $a$-$SiO_2$ structure (black) and for the mesoporous structures with $\rho/\rho_0$=0.88 and pore sizes of 2.5 and 1.25 nm (green and cyan, respectively). In this inset, the smooth curves are quadratic polynomial fits according to the relation $\Delta E \sim (\varepsilon-\varepsilon_0)^2/2$, where $\varepsilon_0$ is the strain at the minimum of the corresponding parabola; $\varepsilon_0$=0 in every case shown except for the one with $d$=1.25 nm. The inset in (b) shows the density dependence of the predicted (open circles) elastic (Young) moduli $M$ for the mesoporous $a$-$SiO_2$ structures with a pore size of 10 nm in a logarithmic plot of $M/M_0$ as a function of $\rho/\rho_0$. The straight line is a fit according to the scaling relationship $M/M_0 \sim (\rho/\rho_0)^\alpha$ with $\alpha$=0.51.

tions according to the power-law scaling relationship $M/M_0 \sim (\rho/\rho_0)^\alpha$. We find an excellent fit for a sublinear ($0<\alpha<1$) power law with an exponent $\alpha$=0.51. This result is in very good agreement with recent experimental data for modulus-density relationships in ordered (cubic) mesoporous silica structures.[6] Figures 2(a) and 2(b) show the dependence of $M$ on $d$ for various densities and of $M$ on $\rho$ for various pore sizes, respectively. These results indicate that at a given density, there is a critical pore diameter $d_c$, which marks the onset of structural instability, i.e., the structural response to straining becomes unstable for $d<d_c$. In a similar manner, at a given pore size, there is a critical density $\rho_c$ such that the structural response of the mesoporous $a$-$SiO_2$ to compressive mechanical straining/loading becomes unstable for $\rho<\rho_c$. It is evident from Figs. 2(a) and 2(b) that $d_c$ decreases with increasing $\rho$ and $\rho_c$ increases with decreasing $d$.

In summary, using MD simulations, we analyzed the mechanical behavior and structural stability of mesoporous amorphous silicas with a regular array of spherical pores over a broad range of densities and pore sizes. We found a sublinear power-law dependence of the Young modulus on density at given pore size and a monotonic decrease of the modulus with decreasing pore size at given density. Our study reveals that upon uniaxial compression, a structural instability may be triggered that is associated with a vanishing Young modulus. The instability originates due to the thinner-than-critical walls between pores, where wall thickness is determined by the combination of pore diameter and density, in the ordered network of mesopores and may lead to pore wall severance, pore coalescence, and rupture of the amorphous mesoporous material. The wall thickness is determined fully by the density and pore diameter. Over the parameter range examined, the onset of this elastic instability can be determined through a critical density that is a monotonically decreasing function of pore diameter $\rho_c(d)$ or a critical pore diameter that is a monotonically decreasing function of density $d_c(\rho)$. The wall thickness $h_w$ is a strong function of pore diameter and the elastic modulus dependence on $h_w$ resembles the results of Fig. 2(a) for the range of parameters examined in our study. A more systematic study of critical behavior as a function of $h_w$ will be presented in a forthcoming publication. Our analysis can be extended to various pore arrangements, such as hexagonal or disordered, various modes of mechanical loading, and various candidate materials and mesoporous materials synthesis methods. The results of such analyses can be instrumental in the development of experimental protocols and materials design strategies toward improving the function of ultralow-$k$ dielectric materials in future generations of microelectronic technologies.

Fruitful discussions with Professor F. Milstein are gratefully acknowledged. This work was supported by the National Science Foundation through Grant Nos. CTS-0304159, CTS-0417770, and DMI-0531171.

[1] R. D. Miller, Science **286**, 421 (1999).
[2] C. L. Wang, M. H. Weber, and K. G. Lynn, J. Appl. Phys. **99**, 113514 (2006).
[3] B. D. Vogt, R. A. Pai, H.-J. Lee, R. C. Hedden, C. L. Soles, W.-l. Wu, E. K. Lin, B. J. Bauer, and J. J. Watkins, Chem. Mater. **17**, 1398 (2005).
[4] R. A. Pai, R. Humayun, M. T. Schulberg, A. Sengupta, J.-N. Sun, and J. J. Watkins, Science **303**, 507 (2004).
[5] Y. Lu, R. Ganguli, C. A. Drewien, M. T. Anderson, C. Brinker, W. Gong, Y. Guo, H. Soyez, B. Dunn, M. Huang, and J. I. Zink, Nature (London) **389**, 364 (1997).
[6] H. Fan, C. Hartshorn, T. Buchheit, D. Tallant, R. Assink, R. Simpson, D. J. Kissel, D. J. Lacks, S. Torquato, and C. J. Brinker, Nat. Mater. **6**, 418 (2007).
[7] Z. Lu, K.-I. Nomura, A. Sharma, W. Wang, C. Zhang, A. Nakano, R. Kalia, P. Vashishta, E. Bouchaud, and C. Rountree, Phys. Rev. Lett. **95**, 135501 (2005).
[8] Y.-C. Chen, Z. Lu, K.-I. Nomura, W. Wang, R. K. Kalia, A. Nakano, and P. Vashishta, Phys. Rev. Lett. **99**, 155506 (2007).
[9] A. Nakano, L. Bi, R. K. Kalia, and P. Vashista, Phys. Rev. Lett. **71**, 85 (1993).
[10] M. Rarivomanantsoa, P. Jund, and R. Jullien, J. Phys.: Condens. Matter **13**, 6707 (2001).
[11] Q. R. Huang, W. Volksen, E. Huang, M. Toney, C. W. Frank, and R. D. Miller, Chem. Mater. **14**, 3676 (2002).
[12] D. Zhao, Q. Huo, J. Feng, B. F. Chmelka, and G. D. Stucky, J. Am. Chem. Soc. **120**, 6024 (1998).
[13] A. Nakano, L. Bi, R. K. Kalia, and P. Vashista, Phys. Rev. B **49**, 9441 (1994).
[14] P. Vashista, R. K. Kalia, and J. P. Rino, Phys. Rev. B **41**, 12197 (1990).
[15] M. P. Allen and D. J. Tildesley, *Computer Simulation of Liquids* (Oxford University Press, Oxford, 1987).
[16] F. Milstein, in *Handbook of Materials Modeling*, edited by S. Yip (Springer, Dordrecht, 2005), p. 1223, and references therein.